Hindawi Publishing Corporation
Journal of Nanomaterials
Volume 2013, Article ID 565074, 11 pages
http://dx.doi.org/10.1155/2013/565074

Research Article

Preparation and Characterization of Highly Efficient and Stable Visible-Light-Responsive Photocatalyst $AgBr/Ag_3PO_4$

Zhang Jinfeng[1] and Zhang Tao[2]

[1] *Department of Physics, Huaibei Normal University, Huaibei, Anhui 235000, China*
[2] *School of Chemistry and Material Science, Huaibei Normal University, Huaibei, Anhui 235000, China*

Correspondence should be addressed to Zhang Tao; 2307382466@qq.com

Received 22 May 2013; Revised 3 August 2013; Accepted 4 August 2013

Academic Editor: Huogen Yu

$AgBr/Ag_3PO_4$ photocatalyst was synthesized using a facile coprecipitation method. The photocatalyst was characterized by X-ray powder diffraction (XRD), UV-Vis diffuse reflectance spectroscopy (DRS), scanning electron microscopy (SEM), Brunauer-Emmett-Teller (BET) surface areas, and photoluminescence (PL) technique. The activity of the photocatalyst was evaluated by the degradation of methyl orange (MO) and rhodamine B (RhB). The results showed that the prepared $AgBr/Ag_3PO_4$ exhibited excellent performance and much higher photocatalytic activity than the single one under visible-light irradiation. The optimum mole ratio of Br/P in $AgBr/Ag_3PO_4$ samples is 0.3. The prepared $AgBr/Ag_3PO_4$ photocatalyst was transformed to $Ag/AgBr/Ag_3PO_4$ system with excellent property and good stability in the photocatalytic process. The possible mechanisms of the enhanced photocatalytic activity for the $AgBr/Ag_3PO_4$ were also discussed in detail.

1. Introduction

Photocatalysis is a promising technology for the treatment of contaminants, especially for the removal of organic pollutants with solar energy [1–6]. To date, TiO_2 has undoubtedly been proven to be the most excellent photocatalyst for the decomposition of many organic compounds. However, TiO_2 photocatalyst has a wide bandgap (i.e., 3.2 eV for anatase and 3.0 eV for rutile) and hence absorbs only the UV light, which accounts for only 4% of the total sunlight, to generate charge carriers for promoting the surface redox reactions. Due to this inherent property of TiO_2 [7–14], its practical applications are rather limited. To effectively utilize the visible light that constitutes 43% of the total sunlight, it is important to find a photocatalyst that is active and efficient under visible-light illumination [15]. Consequently, much effort has been devoted to developing visible-light-driven photocatalysts in order to utilize solar energy and indoor light efficiently in current photocatalysis research field.

Silver halides (AgX, X = Cl, Br, I) are photosensitive materials extensively used as source materials in photographic films. When absorbing a photon, silver halide particle may generate an electron and a hole, so AgX can be used as a potential photocatalyst. But the photoinduced electrons will combine with interstitial Ag^+ ions to form a cluster of Ag^0 atoms within the silver halide particle, which results in the instability of AgX under light irradiation [16]. Therefore, pure AgX is seldom used as a photocatalyst. Recently, Kakuta et al. [17] observed that Ag^0 species are formed on the surface of AgBr in the early stage of the reaction and AgBr in the $AgBr/SiO_2$ photocatalyst is not destroyed under successive UV illumination. The separation of the photoexcited electron-hole pairs may occur in the presence of Ag^0 species on the surface of the photocatalyst. It is considered that the silver nanoparticles formed on silver halide particles might be expected to be a stable photocatalyst under visible-light illumination. At the same time, Ag^0 species formed on the surface of the photocatalysts may produce the effect of surface plasmon resonance (SPR) [15, 18]. Since the results were reported by Kakuta et al. [17], to improve the photostability of AgX, numerous studies have attempted to form composite photocatalysts by loading AgX particles on different materials, such as SiO_2 [19], TiO_2, Al_2O_3 [20–22], Al-MCM-41 [23], Y-zeolite [24], Fe_3O_4 [25], BiOI [26], H_2WO_4 [27, 28], and

Bi_2WO_6 [29, 30]. The results showed that the Ag^0 species on the surface of the catalyst indeed enhanced the interfacial charge transfer and the stability of AgX. This expectation leads us to prepare a new stable photocatalyst under visible-light, which will greatly improve its current performance and open up new applications.

Recently, Ag_3PO_4 has attracted considerable attention as a new visible-light photocatalyst, and it is a pale yellow semiconductor with a bandgap of 2.45 eV [16, 31–33]. The results in the pieces of literature demonstrated that Ag_3PO_4 was a potential photocatalyst in decomposing organics and exhibited outstanding oxygen evolution rate and excellent antibacterial activity under visible-light irradiation. It is known that the conduction band (CB) and valence band (VB) levels of AgBr (2.50 eV) [34] are 0.06 eV and 2.56 eV, respectively, and the CB and VB of Ag_3PO_4 (2.45 eV) are 0.45 eV and 2.90 eV [16, 31], respectively. It is clear that the CB and VB of Ag_3PO_4, respectively, lie below those of AgBr, which is favorable for the efficient separation of photoinduced electrons and holes. Furthermore, $AgBr/Ag_3PO_4$ can be easily transformed into an $Ag/AgBr/Ag_3PO_4$ system in the early stage of the photocatalytic reaction, in which Ag nanoparticles will play an important role. So, AgBr is considered to be an appropriate choice to improve the photocatalytic activity for the Ag_3PO_4 photocatalyst. To the best of our knowledge, however, the study of the composite photocatalyst $AgBr/Ag_3PO_4$ has rarely been reported.

In the study, a novel $AgBr/Ag_3PO_4$ was constructed and synthesized by a facile coprecipitation method. Methyl orange (MO) and rhodamine B (RhB) were used as model pollutants to evaluate the photocatalytic activity of the $AgBr/Ag_3PO_4$ composites under visible-light irradiation ($\lambda > 400$ nm). The optimum mole ratio of Br/P in $AgBr/Ag_3PO_4$ system and the stability of the photocatalyst were also investigated. More importantly, different scavengers were introduced to the photocatalytic reaction system to explore the roles of different reactive species, and the reaction mechanism was discussed in detail.

2. Experimental

2.1. Chemicals and Materials. All reagents are of analytical purity and were used without further purification. Silver nitrate ($AgNO_3$), potassium bromide (KBr), disodium hydrogen phosphate (Na_2HPO_4), methyl orange (MO), rhodamine B (RhB), absolute ethanol, terephthalic acid (TA), benzoquinone (BQ), isopropanol (IPA), potassium iodide (KI), and sodium hydroxide (NaOH) were obtained from Sinopharm Chemical Reagent Co., Ltd. Deionized water was used throughout this study.

2.2. Preparation of $AgBr/Ag_3PO_4$ Photocatalyst. $AgBr/Ag_3PO_4$ was prepared by the coprecipitation method in a dark room to facilitate the experimental manipulation and prevent the decomposition of AgBr. In a typical procedure, 1.42 g of Na_2HPO_4 dispersed in 500 mL of deionized water was placed in a 1000 mL pyrex glass beaker. Then, 0.119 g of KBr in 100 mL of deionized water was added to the above suspension and stirred magnetically for 2 h. Subsequently, 5.3 g of $AgNO_3$ in 100 mL of deionized water was quickly added to the mixture. The resulted suspension was vigorously stirred for 12 h. The product was filtered and washed with absolute ethanol and deionized water for several times and dried at 60°C for 24 h. Finally, the obtained 0.10-$AgBr/Ag_3PO_4$ with theoretical Br/P molar ratio of 0.10 : 1 was collected. Varying the amount of AgBr, different $AgBr/Ag_3PO_4$ photocatalysts were prepared, respectively, and defined as BP-0.1, BP-0.3, BP-0.5, and BP-0.7. Pure Ag_3PO_4 and AgBr samples were prepared using the same method but with only one kind of anion in the solution (PO_4^{3-} or Br^-).

2.3. Characterization of $AgBr/Ag_3PO_4$ Photocatalyst. X-ray diffraction (XRD) measurements were carried out at room temperature using a BRUKER D8 ADVANCE X-ray powder diffractometer with Cu K_α radiation ($\lambda = 1.5406$ Å) and a scanning speed of 3°/min. The accelerating voltage and emission current were 40 kV and 30 mA, respectively. X-ray photoelectron spectroscopy (XPS) examination was carried out on a Thermo ESCALAB 250 multifunctional spectrometer (VG Scientific, UK) using Al Kα radiation. All XPS spectra were referenced to the C1s peak at 284.8 eV from the adventitious hydrocarbon contamination. JEOL JSM-6610LV scanning electron microscope (SEM) with 20 kV scanning voltages was employed to observe the morphologies of as-prepared catalysts. UV-Vis diffuse reflectance spectroscopy (DRS) measurements were carried out using a UV 3600 (SHIMADZU, Japan) UV-Vis-NIR spectrophotometer equipped with an integrating sphere attachment. The analysis range was from 200 to 700 nm, and $BaSO_4$ was used as a reflectance standard. Fluorescence emission spectra were recorded on a JASCO FP-6500 type fluorescence spectrophotometer with 315 nm excited source over a wavelength range of 350–600 nm. The Brunauer-Emmett-Teller (BET) surface areas were measured using a Micromeritics ASAP 2020 N_2-physisorption method at 77 K.

2.4. Photocatalytic Activity Test. The photocatalytic degradations of MO and RhB were adopted to evaluate the photocatalytic activity of the samples in a photoreaction apparatus [35]. A 500 W Xe lamp (Institute of Electric Light Source, Beijing) was used as a light source with a 400 nm cut-off filter (Instrument Company of Nantong, China) to provide visible-light irradiation. In each experiment, the reaction suspension containing 0.05 g photocatalyst and 25 mL dye solution was put in the 100 mL beaker, and a magnetic stirrer was used to stir the reaction solution. The initial concentrations of MO and RhB were 10 mg/L and 4.0 mg/L, respectively. And the initial pH value of solution is 7.0. The distance between the light source and the surface of the reaction solution is 11 cm. Prior to illumination, the suspension was magnetically stirred in the dark for 30 min to reach adsorption-desorption equilibrium of the dyes on catalyst surfaces. At the given time intervals, 5 mL of the suspension was collected, centrifuged, and filtered through a 0.2 μm millipore filter to

remove the catalyst particles. The concentration of catalyst-free dye solution is determined spectrophotometrically. The photocatalytic activity of the samples is calculated from the following expression [35]:

$$\eta = \left[\frac{(C_0 - C)}{C_0}\right] \times 100\%, \quad (1)$$

where η is the photocatalytic efficiency; C_0 is the concentration of reactant before illumination (mg/L); C is the concentration of reactant after illumination time t (mg/L).

3. Results and Discussion

3.1. Characterization of $AgBr/Ag_3PO_4$ Photocatalyst

3.1.1. XRD Analysis. In order to determine the crystal phase composition and the crystallite size of the photocatalyst, XRD study of the samples was carried out. Figure 1 shows the XRD patterns of different photocatalysts. The patterns show that Ag_3PO_4 is a body-centered cubic structure (JCPDS no. 06-0505) and AgBr is face-centered cubic crystal (JCPDS no. 06-0438). The result is in accordance with the previous report [16]. As shown in Figure 1, it can be seen that when the amount of AgBr is 0.1, the diffraction peaks of AgBr can be found in XRD patterns. And with further increase of AgBr concentration, the intensity of diffraction peaks of AgBr increases remarkably, whereas the intensity of diffraction peaks of Ag_3PO_4 decreases simultaneously. It demonstrates that the AgBr particles are evenly dispersed on the surface of Ag_3PO_4 particles. The calculation from the Scherrer equation shows that the diameter of Ag_3PO_4 in the composite photocatalyst is not obviously changed compared with that of pure Ag_3PO_4. The average crystallite size of Ag_3PO_4 is about 30 nm according to the main peak (210) of Ag_3PO_4, and the calculated crystallite size of AgBr is about 53.5 nm according to the main peak (200) of AgBr. No other new crystal phases are found in the patterns. In addition, XRD analysis was also carried out for the used $AgBr/Ag_3PO_4$ photocatalyst. The result is shown in Figure 2. It is clear that a new diffraction peak at 38.07° (JCPDS no. 04-0783) assigned to Ag was found in the used BP0.1 after one and five recycling runs compared with the fresh BP0.1. However, the diffraction peak at 38.07° is not obviously changed between the sample used one time and five times. It is suggested that the photocatalyst is stable in the experimental conditions. The color of the fresh photocatalyst is faint yellow, and the color of the used photocatalyst becomes a little darker. This demonstrates that the fresh $AgBr/Ag_3PO_4$ photocatalyst has been changed into $Ag/AgBr/Ag_3PO_4$ photocatalyst after photocatalytic reaction.

3.1.2. XPS Analysis. To further confirm the existence of Ag in the used $AgBr/Ag_3PO_4$ sample, the used BP-0.1 sample was examined by XPS. The results are shown in Figure 3. Figure 3(a) displays the XPS survey spectrum of the used $AgBr/Ag_3PO_4$ photocatalyst, which mainly exhibits the peaks of Ag, Br, P, O, and C. The XPS peak for C1s (284.8 eV) is ascribed to the adventitious hydrocarbon from the XPS instrument. In addition, no other impurity is found in the

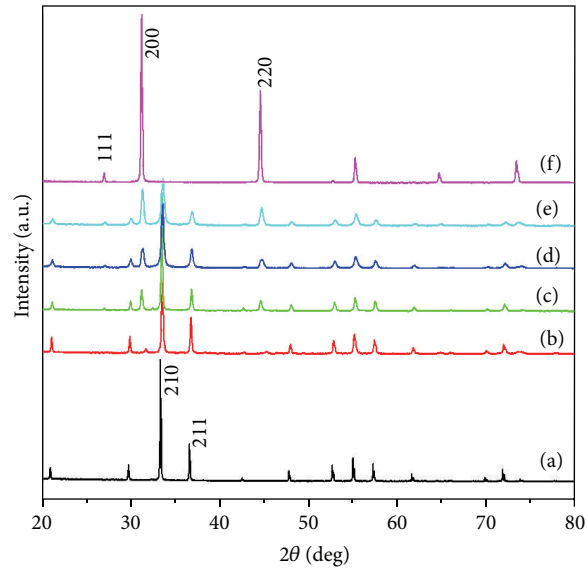

Figure 1: XRD patterns of (a) Ag_3PO_4, (b) BP-0.1, (c) BP0.3, (d) BP-0.5, (e) BP-0.7, and (f) AgBr.

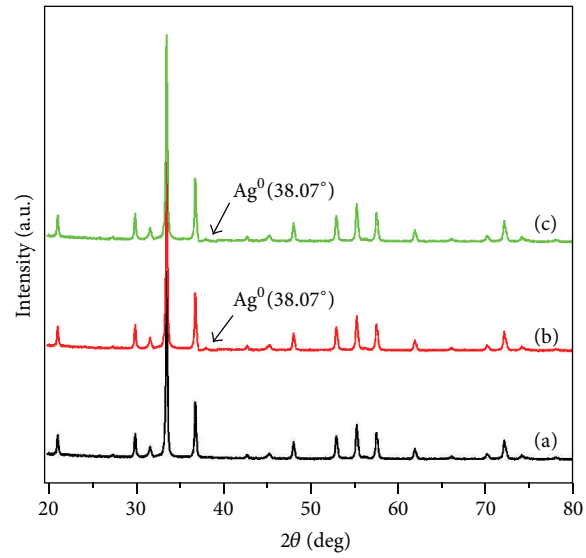

Figure 2: XRD patterns of (a) fresh BP0.1, (b) used one time BP0.1 and (c) used five times BP-0.1.

sample. A typical high-resolution XPS spectrum of Ag 3d is shown in Figure 3(b). The Ag 3d spectrum of $AgBr/Ag_3PO_4$ is made up of two individual peaks at 374 and 368 eV, which can be attributed to the binding energies of Ag $3d_{3/2}$ and Ag $3d_{5/2}$, respectively. The Ag $3d_{3/2}$ peak is further divided into two different peaks at 374.15 and 375.2 eV, and the Ag $3d_{5/2}$ peak is divided into two different peaks at 368.15 and 369.15 eV, respectively. The peaks at 375.2 and 369.15 eV are attributed to metal Ag^0, and the peaks at 374.15 and 368.15 eV are attributed to Ag^+ of AgBr and Ag_3PO_4 [36]. From the result, it is clear that the metal Ag should have been formed on the surface of the $AgBr/Ag_3PO_4$ photocatalyst in the reaction.

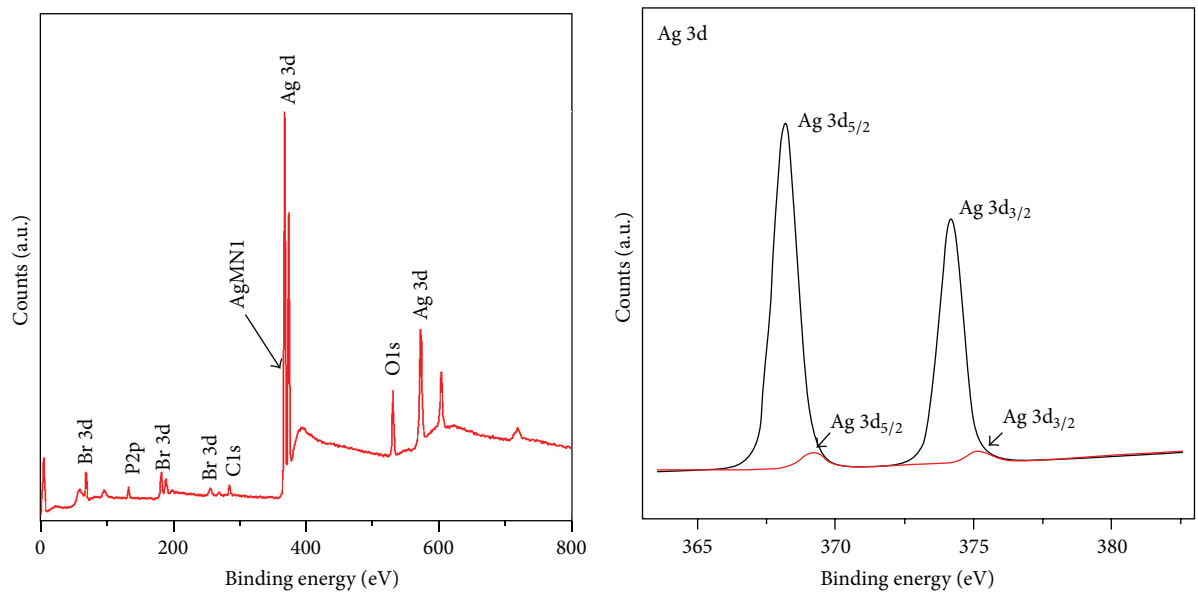

Figure 3: XPS survey spectrum (a) and Ag 3d XPS spectrum (b) of the used $AgBr/Ag_3PO_4$.

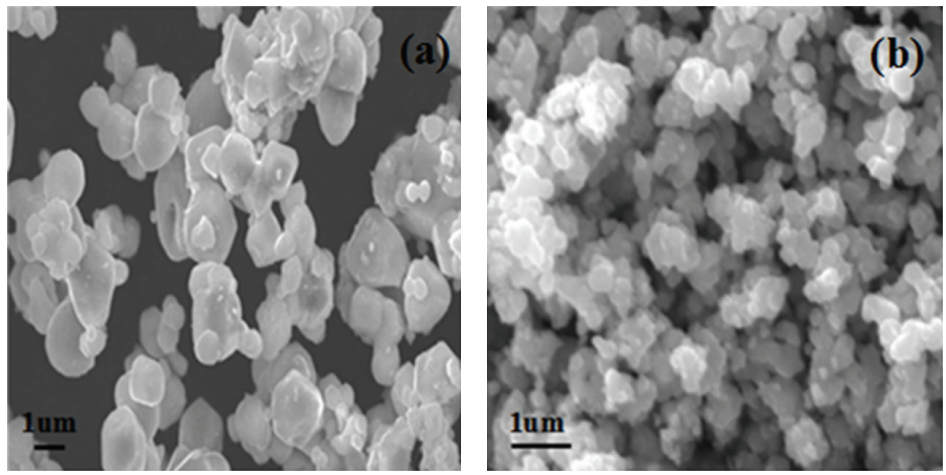

(a) (b)

Figure 4: SEM images of (a) Ag_3PO_4 and (b) $AgBr/Ag_3PO_4$ (BP-0.3).

3.1.3. SEM Analysis. SEM was used to investigate the morphology of the photocatalysts. Figure 4 shows the SEM photographs of the Ag_3PO_4 and $AgBr/Ag_3PO_4$ (BP-0.3), respectively. It can be seen that the appearance of the Ag_3PO_4 photocatalyst in Figure 4(a) is irregular spheroidal structure with mean size of about 1 μm. The appearance of $AgBr/Ag_3PO_4$ is shown in Figure 4(b). It is clear that AgBr is highly dispersed on the surface of the photocatalyst, and it is composed of many small nanoparticles, and their average particle sizes are about 200 nm.

3.1.4. DRS Analysis. UV-Vis diffuse reflectance spectroscopy was carried out to investigate the optical properties of the samples. Figure 5 shows UV-Vis diffuse reflectance spectra of different photocatalysts. From Figure 5(a), it can be seen that, compared with pure AgBr, the absorption wavelength range of the BP-0.3 photocatalyst is extended greatly towards visible light. In theory, because the absorption wavelength range is extended greatly towards visible light, the formation rate of electron-hole pairs on the photocatalyst surface also increases greatly, resulting in the photocatalyst exhibiting higher photocatalytic activity. The absorption wavelength range of the BP-0.3 photocatalyst is extended greatly towards visible light, which may be attributed to the formation of the heterojunction between AgBr and Ag_3PO_4. A similar result was also reported [37].

From Figure 5(a), it is clear that the absorption edge of the prepared Ag_3PO_4 and AgBr samples is at about 506 nm

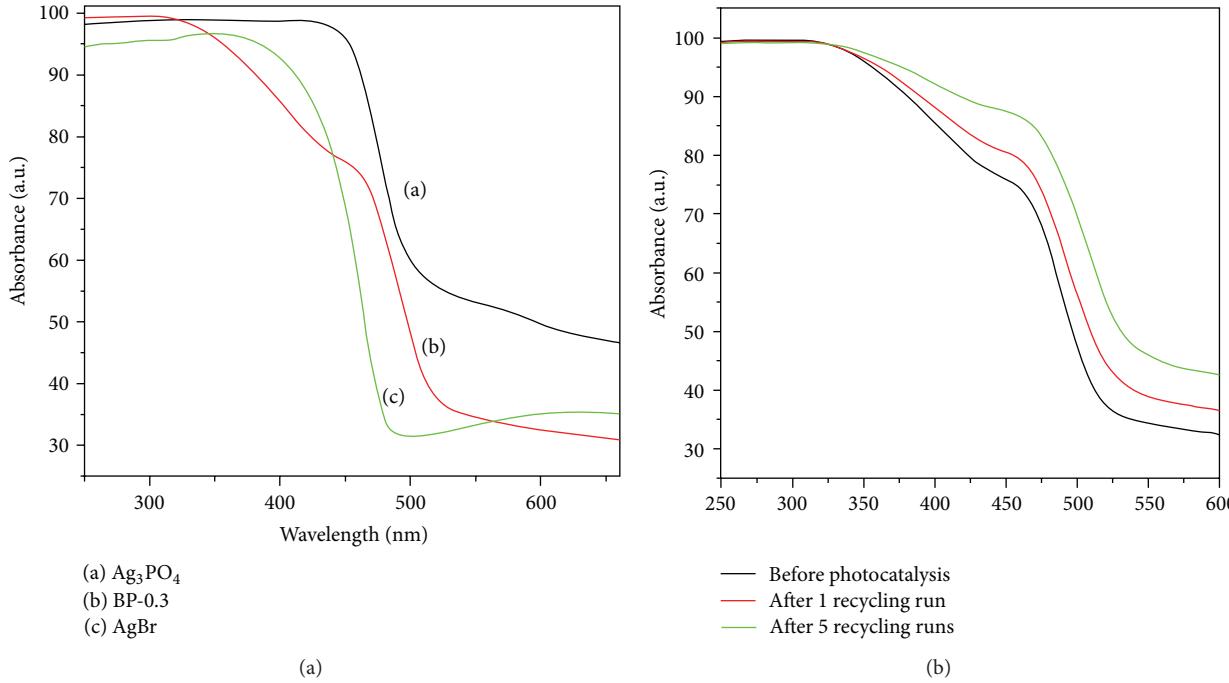

(a) (b)

FIGURE 5: (a) DRS of AgBr, Ag_3PO_4, and BP-0.3 samples. (b) DRS of the fresh BP-0.3, the used one time BP-0.3, and the used five times BP-0.3.

and 496 nm in the spectrum, respectively. It is known that the bandgap energy of the photocatalysts can be calculated by the following equation [38, 39]:

$$\alpha h\nu = A(h\nu - E_g)^{n/2}. \quad (2)$$

In this equation, α, h, ν, A, and E_g are absorption coefficient, Planck constant, light frequency, proportionality, and bandgap energy, respectively; n is determined from the type of optical transition of a semiconductor ($n = 1$ for direct transition and $n = 4$ for indirect transition). The values of n for AgBr and Ag_3PO_4 are 4 [40] and 1 [41], respectively. By applying this equation, the bandgap of AgBr and Ag_3PO_4 is 2.50 eV and 2.45 eV, respectively, which agrees well with the previous reports [16, 31, 32, 34].

The band edge positions of CB and VB of semiconductor can be determined with a simple approach. The valance band edge (E_{VB}) and conduction band edge (E_{CB}) of a semiconductor at the point of zero charge (pH_{ZPC}) can be predicted by the following equation [42]:

$$E_{VB} = X - E_e + 0.5E_g$$
$$E_{CB} = E_{VB} - E_g, \quad (3)$$

where X is the absolute electronegativity of the semiconductor, expressed as the geometric mean of the absolute electronegativity of the constituent atoms, which is defined as the arithmetic mean of the atomic electron affinity and the first ionization energy. E_e is the energy of free electrons on the hydrogen scale (likely 4.5 eV), and E_g is the bandgap energy of the semiconductor. The X values for AgBr and Ag_3PO_4 are 5.81 and 6.17 eV, and the E_{VB} of AgBr and Ag_3PO_4 are calculated to be 2.56 and 2.9 eV, respectively. Thus, the E_{CB} of AgBr and Ag_3PO_4 are estimated to be 0.06 and 0.45 eV, respectively. The UV-Vis diffuse reflectance spectra of the used photocatalyst (BP-0.3) are shown in Figure 5(b). It is clear that, compared with the fresh BP0.3 photocatalyst, there is much stronger absorption in the visible region, and with the increase in the recycling runs, the absorption wavelength range and the absorption intensity increase gradually. It may be resulted from the strong surface plasmon resonance (SPR) [43, 44] effect of Ag nanometer particles (NPs) scattering on the surface of AgBr and Ag_3PO_4 particles. The gradually enhanced absorption in the visible region from 1 to 5 recycling runs shows that the amount of Ag NPs increases slowly in the photocatalytic reaction. The increased content of metal Ag will affect the size of Ag, which further affects the separation of photoinduced carriers, the SPR effect of Ag NPs, and the corresponding photocatalytic activities [15].

3.2. Photocatalytic Activity of $AgBr/Ag_3PO_4$

3.2.1. Degradation of Dyes. The photocatalytic activities of as-prepared samples were evaluated by the degradation of MO and RhB under visible-light irradiation. The blank test shows that photoinduced self-sensitized photodegradation has little influence on the results of the experiment. At the same time, the dark absorption test in the absence of irradiation but with the catalysts shows that no significant change in the substrate concentration is found.

Figure 6(a) displays the degradation of MO by the different photocatalysts. It is clear that the BP-0.3 photocatalyst exhibits the highest catalytic activity. The degradation efficiency of MO is 56.3%, 60.2%, 89.8%, 82.3%, and 78.2% for

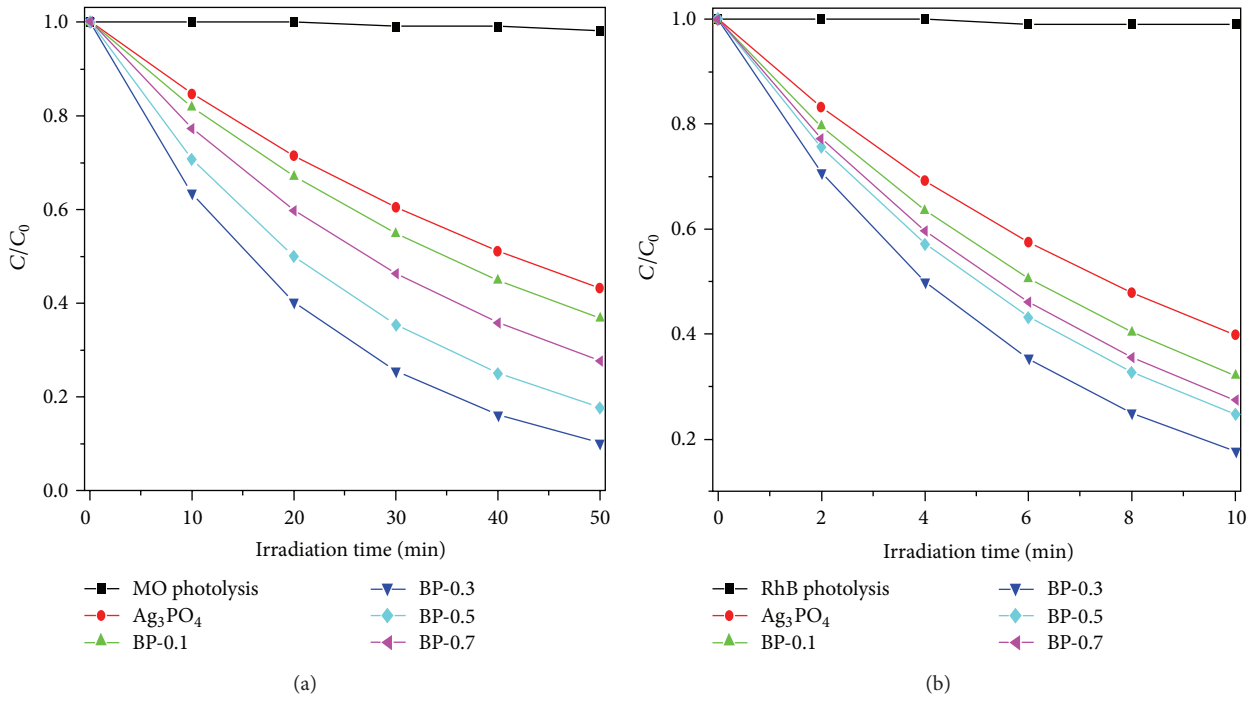

FIGURE 6: (a) The degradation process of MO with different photocatalysts. (b) The degradation process of RhB with different photocatalysts.

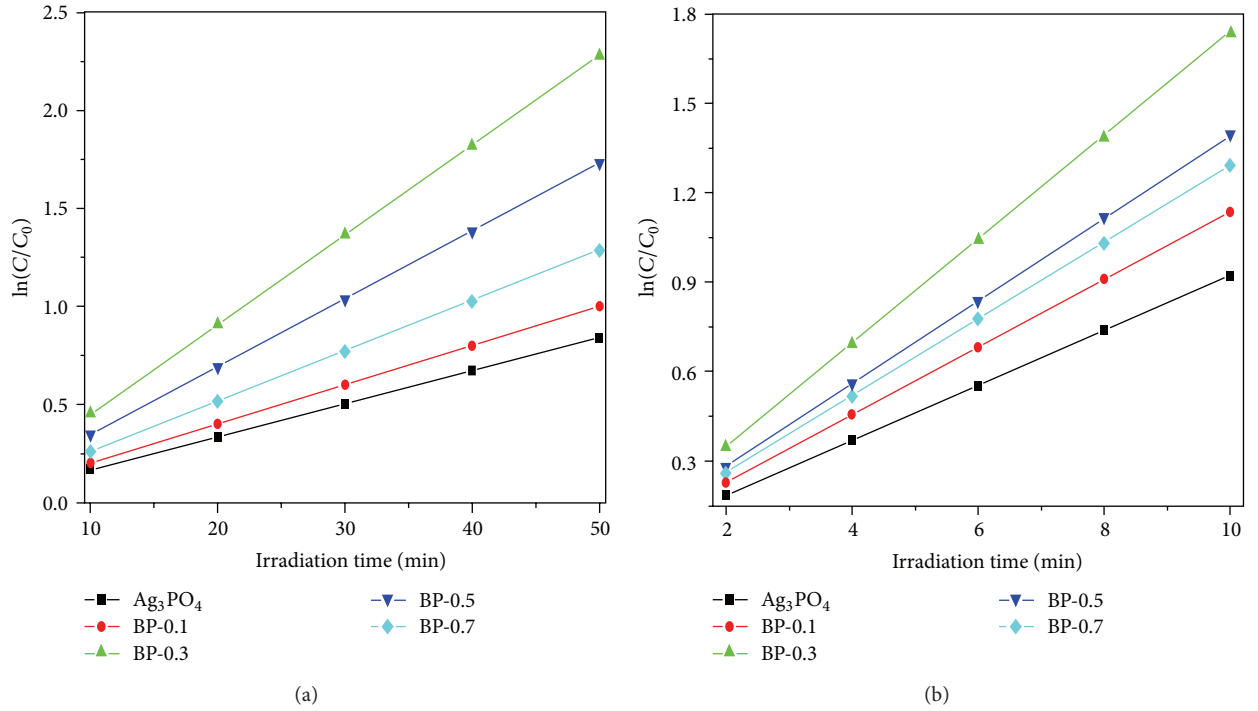

FIGURE 7: (a) The first-order kinetics of MO degradation with different photocatalysts. (b) The first-order kinetics of RhB degradation with different photocatalysts.

Ag_3PO_4, BP-0.1, BP-0.3, BP-0.5, and BP-0.7 after irradiation for 50 min, respectively. For the degradation of RhB, a similar change tendency of degradation efficiency is also displayed in Figure 6(b) as that of MO degradation. When illuminated for 10 min, the degradation efficiency of RhB is 60.2%, 67.9%, 82.4%, 75.3%, and 72.6% for Ag_3PO_4, BP-0.1, BP-0.3, BP-0.5, and BP-0.7, respectively.

Figures 7(a) and 7(b) show the kinetics of MO and RhB photocatalytic degradation with different photocatalysts, respectively. It is clear that the photocatalytic degradation

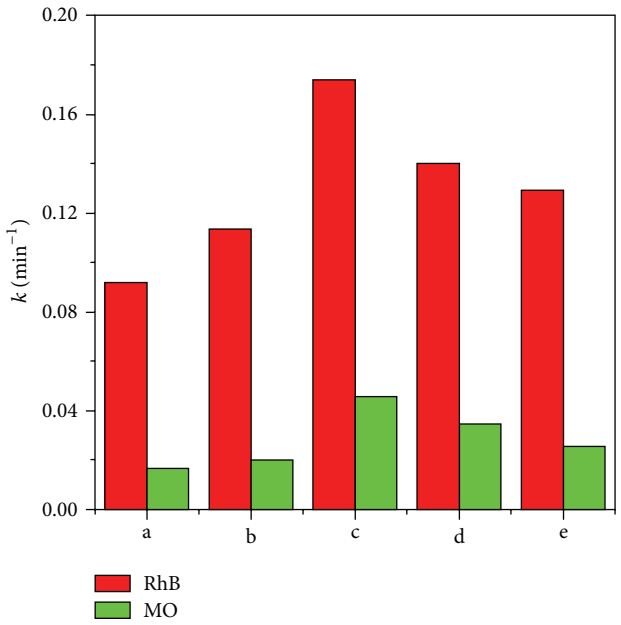

FIGURE 8: The rate constants of MO and RhB degradation with different samples: Ag_3PO_4 (a), BP-0.1 (b), BP-0.3 (c), BP-0.5 (d) and BP-0.7 (e).

process of MO and RhB follows first-order kinetics equation. According to the kinetics model, the rate constant k of the different Ag_3PO_4/AgBr samples and pure Ag_3PO_4 is calculated and illustrated in Figure 8. The results demonstrate that the optimum sample is BP-0.3 with the maximal degradation rate constant of 0.1737 min^{-1} for RhB and 0.0456 min^{-1} for MO, which is about 2 and 3 times that of pure Ag_3PO_4, respectively.

The BET surface areas of Ag_3PO_4, BP-0.1, BP-0.3, BP-0.5, and BP-0.7 are 2.3, 2.6, 3.1, 3.7, and 3.7 m^2/g, respectively. It is clear that the BET surface areas of the samples are increased gradually with the increase in the amount of AgBr. It is obvious that the increased photocatalytic activity is not in obvious correspondence with the BET surface area of the samples. Therefore, the enhanced photocatalytic activity of the samples can only be ascribed to the presence of AgBr.

3.2.2. Stability of the Photocatalyst. The catalyst's lifetime is an important parameter of the photocatalytic reaction process, so it is essential to evaluate the stability of the catalyst for practical application. As shown in Figure 9(a), the repetition tests reveal that the photocatalytic degradation efficiency of MO for BP-0.3 sample decreases by 12.3% after 5-time cycle experiments, and after 2-time cycle experiments, the photocatalytic degradation efficiency of MO is obviously decreased, which indicates that AgBr/Ag_3PO_4 has high stability under visible-light irradiation. The stability of AgBr/Ag_3PO_4 was also studied through the degradation of RhB (Figure 9(b)). The result shows that the photocatalytic activity of AgBr/Ag_3PO_4 is not obviously changed and only little decrease after 5-time cycles. It further confirms the good stability of the AgBr/Ag_3PO_4 photocatalyst. From Figure 9, it is clear that, though AgBr/Ag_3PO_4 is not very stable at the initial reaction process under visible-light irradiation, the formed Ag/AgBr/Ag_3PO_4 system can effectively retain its activity due to the efficient transfer of photoexcited electrons by Ag nanoparticles [45].

The high photocatalytic activity and good stability are closely related to the efficient separation of photoexcited electron-hole pairs derived from the matching band potentials between AgBr and Ag_3PO_4, as well as the surface plasmon resonance of Ag nanoparticles formed on the surface of the photocatalyst during the photocatalytic reaction process. The presence of metal Ag can restrain the further decomposition of AgBr under visible-light irradiation conditions [46, 47]. Besides, Br^0 atoms produced by AgBr under visible-light irradiation are the reactive radical species to degrade MO and RhB and then turn to Br^-, because the holes in the VB of AgBr can oxidize Br^- ions to Br^0 atoms. If the number of Br^0 atoms from AgBr reaches a certain amount, Br^- ions to Br^0 atoms will balance on the surface of the photocatalyst. Consider

$$\begin{aligned} Br^- + h^+ &\longrightarrow Br^0, \\ Br^0 + \text{Dyes} &\longrightarrow Br^-. \end{aligned} \tag{4}$$

Therefore, the obtained AgBr-Ag-Ag_3PO_4 nanojunction photocatalyst is a stable and effective photocatalyst under the experimental conditions.

3.3. Proposed Photocatalytic Mechanism

3.3.1. Roles of Reactive Species. The photocatalytic mechanism was investigated for the excellent photocatalytic property of the prepared AgBr/Ag_3PO_4. It is generally accepted that the dyes and organic pollutants can be photodegraded via photocatalytic oxidation process. A large number of main reactive species including h^+, $^{\bullet}OH$, and $^{\bullet}O_2^-$ are involved in the photocatalytic oxidation process. Therefore, the effects of some scavengers on the degradation of RhB and MO were examined in an attempt to elucidate the reaction mechanism. As an $^{\bullet}O_2^-$ scavenger, benzoquinone (BQ) was added to the reaction system. Isopropanol (IPA) was introduced as the scavenger of $^{\bullet}OH$, and ammonium oxalate (AO) was adopted to quench h^+ [40]. As a consequence of quenching, photocatalytic oxidation reaction is partly suppressed, and η is lowered. The more η is reduced by scavengers, the more important the role the corresponding oxidizing species play in the photocatalytic oxidation reaction. The effects of a series of scavengers on the degradation efficiency of MO and RhB are shown in Figure 10. It can be seen from Figure 6 that the degradation efficiencies of the AgBr/Ag_3PO_4 (BP0.3) photocatalyst for RhB and MO are 82.4% and 89.8%, respectively, before the quenchers are added. However, the photodegradation efficiencies of RhB and MO are reduced to 32.1% and 36.5%, respectively, after adding ammonium oxalate (AO). Adding benzoquinone (BQ), the photodegradation efficiencies for RhB and MO are decreased to 45.3% and 48.2%, respectively. However, there is almost no obvious change for the photodegradation of RhB and MO after mixing

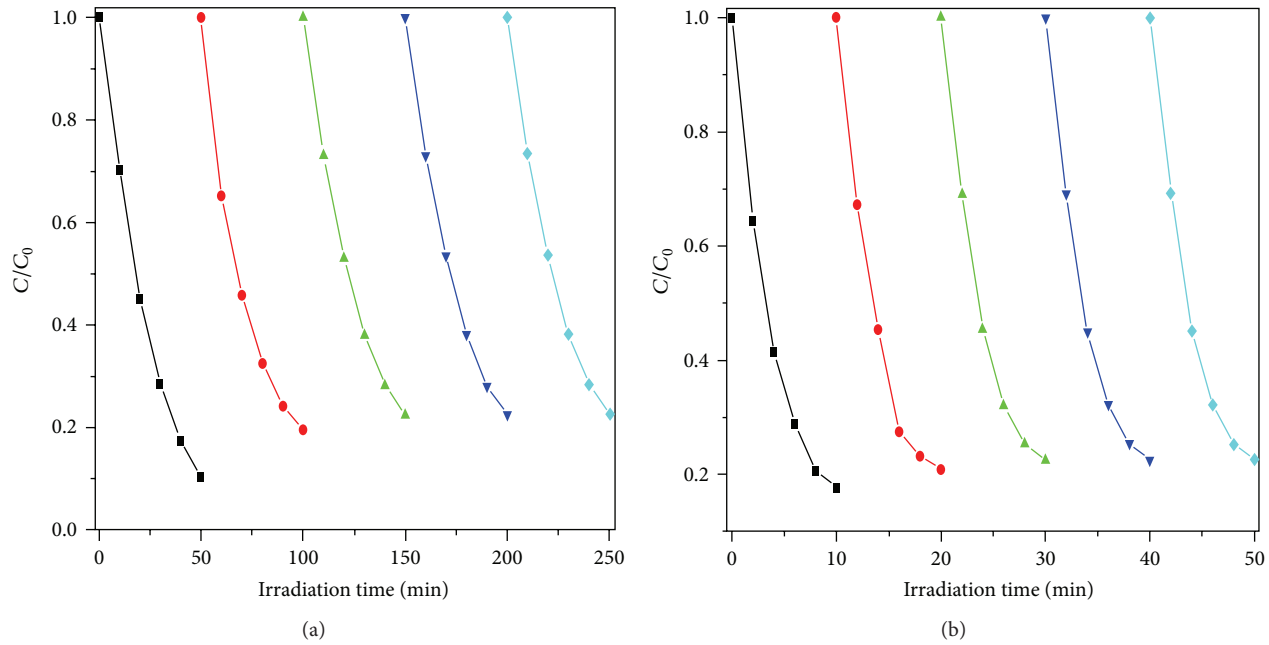

Figure 9: (a) Cyclic experiments of the BP-0.3 photocatalyst for MO degradation. (b) Cyclic experiments of the BP-0.3 photocatalyst for RhB degradation.

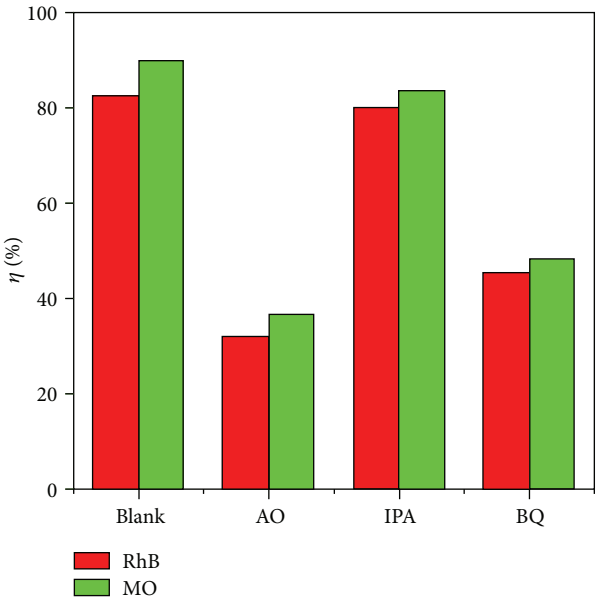

Figure 10: The effects of a series of scavengers on the degradation efficiency of MO and RhB (the dosage of scavengers = 0.1 mmol/L, illumination times are 50 min and 10 min for MO and RhB, resp.).

the isopropanol (IPA). According to the above experimental results, it can be clearly seen that $^{\bullet}O_2^-$ and h^+ are the main reactive species in the photocatalytic oxidation process of RhB and MO, whereas the effect of $^{\bullet}OH$ can be negligible in this process.

To further research whether $^{\bullet}OH$ was formed on the surface of $AgBr/Ag_3PO_4$ (BP-0.3) photocatalyst under visible light illumination, a photoluminescence (PL) technique with terephthalic acid as a probe molecule was carried out. The detailed experimental procedures have been reported in our earlier reports [48, 49]. The PL emission spectra excited at 315 nm from TA solution suspension with $AgBr/Ag_3PO_4$ were measured every 10 min. The results are shown in Figure 11. It can be seen that no obvious PL signal at about 425 nm is observed, demonstrating that no $^{\bullet}OH$ is formed in the photocatalytic oxidation process, which agrees well with the results of IPA quenching. In summary, the main reactive species involved in the degradation of MO (or RhB) are h^+ and $^{\bullet}O_2^-$.

3.3.2. Proposed Mechanism. Based on bandgap structure of the prepared $AgBr/Ag_3PO_4$ and the effects of scavengers, a possible mechanism of $AgBr/Ag_3PO_4$ photocatalyst for degradation dyes was proposed. The $AgBr/Ag_3PO_4$ photocatalyst was transformed into a plasmonic Z-scheme mechanism of $Ag_3PO_4/Ag/AgBr$ system during the photocatalytic oxidation process. In other words, the $AgBr/Ag_3PO_4$ photocatalyst was firstly transformed into the $Ag_3PO_4/Ag/AgBr$ photocatalyst under visible-light irradiation. And then, AgBr, Ag, and Ag_3PO_4 can be simultaneously excited and produce photogenerated electrons and holes. The plasmon-induced electrons of Ag nanoparticles are injected into the CB of AgBr, while the holes remain on the Ag nanoparticles. As for Ag_3PO_4, the photogenerated electrons move to the Ag nanoparticles to recombine with the plasmon-induced holes produced by plasmonic absorption of Ag nanoparticles, while the holes in the VB of Ag_3PO_4 may oxidize MO and RhB directly. Besides, it was reported that electrons in the CB of AgBr could probably be excited up to a higher potential

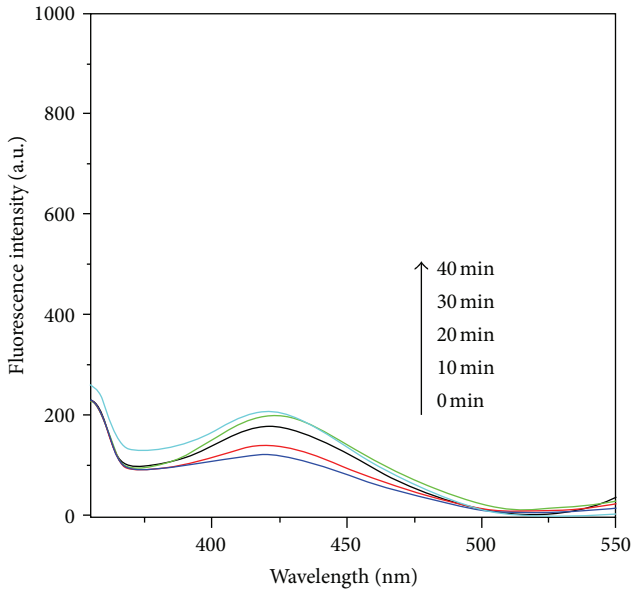

FIGURE 11: The PL spectra of $AgBr/Ag_3PO_4$ in TA solution under visible-light irradiation.

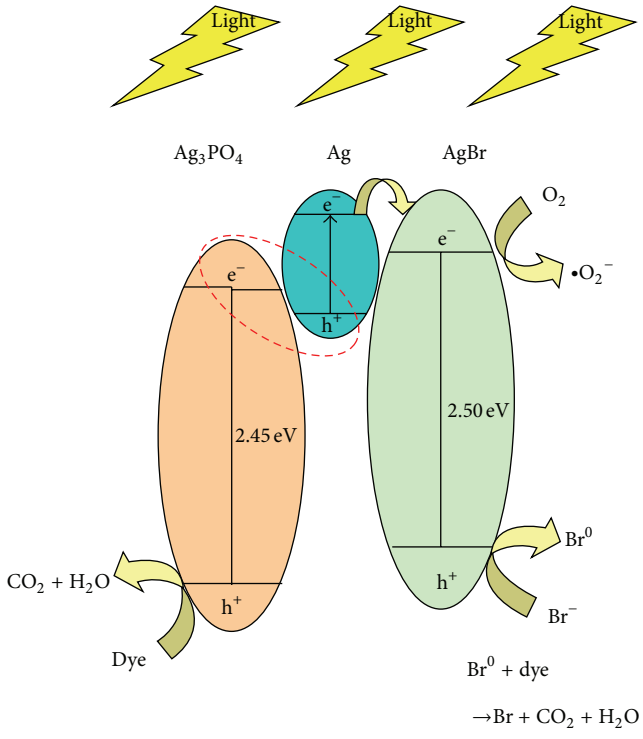

FIGURE 12: Schematic diagram of photoexcited electron-hole separation process.

edge (−0.39 eV) under visible-light illumination with energy less than 2.95 eV [45, 46, 50]. These electrons will further react with O_2 to generate reactive $^{\bullet}O_2^-$ ($E^{\Theta}(O_2/^{\bullet}O_2^-)$ = −0.33 eV versus NHE) that induced the degradation of MO and RhB. The holes in the VB of AgBr oxidize Br^- ions to Br^0 atoms, which are the reactive radical species to degrade MO and RhB. In summary, MO and RhB were decomposed by $Ag/AgBr/Ag_3PO_4$ systems under visible-light irradiation through $^{\bullet}O_2^-$, Br^0, and direct h^+ oxidation pathway. Based on the analyses, the proposed schematic diagram of photoexcited electron-hole separation process is shown in Figure 12.

4. Conclusions

$AgBr/Ag_3PO_4$ photocatalyst was synthesized using a facile coprecipitation method. The prepared $AgBr/Ag_3PO_4$ exhibited excellent performance for the degradation of MO and RhB and displayed a much higher photocatalytic activity than the single one under visible-light irradiation. The optimum mole ratio of Br/P in $AgBr/Ag_3PO_4$ samples is 0.3. The $AgBr/Ag_3PO_4$ photocatalyst was transformed to $Ag/AgBr/Ag_3PO_4$ photocatalyst quickly, and the formed $Ag/AgBr/Ag_3PO_4$ photocatalyst remained with high photocatalytic property and good stability in the photocatalytic process. The reason is attributed to the efficient separation of photoexcited electron-hole pairs of the photocatalyst. The degradation of MO and RhB for the $AgBr/Ag_3PO_4$ photocatalyst is mainly via $^{\bullet}O_2^-$, Br^0, and direct h^+ oxidation process. The $AgBr/Ag_3PO_4$ photocatalyst may be a promising, efficient, and stable photocatalyst for new applications in environmental purification under visible-light irradiation.

Acknowledgment

This study was supported by the Natural Science Foundation of China (NSFC, Grant nos. 20973071, 51172086, 21103060, and 51272081).

References

[1] R. Jiang, H. Zhu, X. Li, and L. Xiao, "Visible light photocatalytic decolourization of C. I. Acid Red 66 by chitosan capped CdS composite nanoparticles," *Chemical Engineering Journal*, vol. 152, no. 2-3, pp. 537–542, 2009.

[2] W. Wang, W. Zhu, and H. Xu, "Monodisperse, mesoporous ZnxCd1-xS nanoparticles as stable visible-light-driven photocatalysts," *Journal of Physical Chemistry C*, vol. 112, no. 43, pp. 16754–16758, 2008.

[3] S. C. Yan, Z. S. Li, and Z. G. Zou, "Photodegradation performance of g-C_3N4 fabricated by directly heating melamine," *Langmuir*, vol. 25, no. 17, pp. 10397–10401, 2009.

[4] J. S. Jang, K. Y. Yoon, Y. Xiao, F.-R. F. Fan, and A. J. Bard, "Development of a potential Fe_2O_3-based photocatalyst thin film for water oxidation by scanning electrochemical microscopy: Effects of Ag-Fe_2O_3 nanocomposite and Sn doping," *Chemistry of Materials*, vol. 21, no. 20, pp. 4803–4810, 2009.

[5] K. Ikcue, S. Shiiba, and M. Machida, "Novel visible-light-driven photocatalyst Based on Mn-Cd-S for efficient H_2 evlution," *Chemistry of Materials*, vol. 22, no. 3, pp. 743–745, 2010.

[6] R. Abe, H. Takami, N. Murakami, and B. Ohtani, "Pristine simple oxides as visible light driven photocatalysts: highly efficient decomposition of organic compounds over platinum-loaded tungsten oxide," *Journal of the American Chemical Society*, vol. 130, no. 25, pp. 7780–7781, 2008.

[7] C. Hu, Y. Lan, J. Qu, X. Hu, and A. Wang, "Ag/AgBr/TiO_2 visible light photocatalyst for destruction of azodyes and bacteria," *Journal of Physical Chemistry B*, vol. 110, no. 9, pp. 4066–4072, 2006.

[8] C. Hu, X. Hu, L. Wang, J. Qu, and A. Wang, "Visible-light-induced photocatalytic degradation of azodyes in aqueous Agl/TiO_2 dispersion," *Environmental Science and Technology*, vol. 40, no. 24, pp. 7903–7907, 2006.

[9] Y. Lan, C. Hu, X. Hu, and J. Qu, "Efficient destruction of pathogenic bacteria with AgBr/TiO_2 under visible light irradiation," *Applied Catalysis B*, vol. 73, no. 3, pp. 354–360, 2007.

[10] M. R. Elahifard, S. Rahimnejad, S. Haghighi, and M. R. Gholami, "Apatite-coated Ag/AgBr/TiO_2 visible-light photocatalyst for destruction of bacteria," *Journal of the American Chemical Society*, vol. 129, no. 31, pp. 9552–9553, 2007.

[11] Y. Zang and R. Farnood, "Photocatalytic activity of AgBr/TiO_2 in water under simulated sunlight irradiation," *Applied Catalysis B*, vol. 79, no. 4, pp. 334–340, 2008.

[12] J. Cao, H.-L. Lin, L. Jia, and S.-F. Chen, "AgBr/TiO_2 composite catalyst: preparation by double-jet method and visible light photocatalytic property," *Yingxiang Kexue yu Guanghuaxue*, vol. 27, no. 6, pp. 462–468, 2009.

[13] C. Hu, J. Guo, J. Qu, and X. Hu, "Photocatalytic degradation of pathogenic bacteria with AgI/TiO_2 under visible light irradiation," *Langmuir*, vol. 23, no. 9, pp. 4982–4987, 2007.

[14] Y. Li, H. Zhang, Z. Guo et al., "Highly efficient visible-light-induced photocatalytic activity of nanostructured AgI/TiO_2 photocatalyst," *Langmuir*, vol. 24, no. 15, pp. 8351–8357, 2008.

[15] P. Wang, B. Huang, X. Zhang et al., "Highly efficient visible-light plasmonic photocatalyst Ag@AgBr," *Chemistry*, vol. 15, no. 8, pp. 1821–1824, 2009.

[16] Z. Yi, J. Ye, N. Kikugawa et al., "An orthophosphate semiconductor with photooxidation properties under visible-light irradiation," *Nature Materials*, vol. 9, no. 7, pp. 559–564, 2010.

[17] N. Kakuta, N. Goto, H. Ohkita, and T. Mizushima, "Silver Bromide as a Photocatalyst for Hydrogen Generation from CH_3OH/H_2O Solution," *Journal of Physical Chemistry B*, vol. 103, no. 29, pp. 5917–5919, 1999.

[18] M. Rycenga, C. M. Cobley, J. Zeng et al., "Controlling the synthesis and assembly of silver nanostructures for plasmonic applications," *Chemical Reviews*, vol. 111, no. 6, pp. 3669–3712, 2011.

[19] N. Kakuta, N. Goto, H. Ohkita, and T. Mizushima, "Nanostructured AgBr loaded TiO_2: an efficient sunlight active photocatalyst for degradation of Reactive Red 120," *The Journal of Physical Chemistry B*, vol. 103, pp. 5917–5919, 1999.

[20] Y. Yamashita, N. Aoyama, N. Takezawa, and K. Yoshida, "Characterization of hightly active AgCl/Al_2O_3 catalyst for photocatalytic conversion of NO," *Environmental Science & Technology*, vol. 34, pp. 5211–5214, 2000.

[21] X. Zhou, C. Hu, X. Hu, T. Peng, and J. Qu, "Plasmon-assisted degradation of toxic pollutants with Ag-AgBr/Al_2O_3 under visible-light irradiation," *Journal of Physical Chemistry C*, vol. 114, no. 6, pp. 2746–2750, 2010.

[22] C. Hu, T. Peng, X. Hu et al., "Plasmon-induced photodegradation of toxic pollutants with Ag-AgI/Al_2O_3 under visible-light irradiation," *Journal of the American Chemical Society*, vol. 132, no. 2, pp. 857–862, 2010.

[23] S. Rodrigues, S. Uma, I. N. Martyanov, and K. J. Klabunde, "AgBr/Al-MCM-41 visible-light photocatalyst for gas-phase decomposition of CH_3CHO," *Journal of Catalysis*, vol. 233, no. 2, pp. 405–410, 2005.

[24] Y. Zang, R. Farnood, and J. Currie, "Photocatalytic activities of AgBr/Y-zeolite in water under visible light irradiation," *Chemical Engineering Science*, vol. 64, no. 12, pp. 2881–2886, 2009.

[25] G. Li, K. H. Wong, X. Zhang et al., "Degradation of Acid Orange 7 using magnetic AgBr under visible light: the roles of oxidizing species," *Chemosphere*, vol. 76, no. 9, pp. 1185–1191, 2009.

[26] H. Cheng, B. Huang, Y. Dai, X. Qin, and X. Zhang, "One-step synthesis of the nanostructured AgI/BiOI composites with highly enhanced visible-light photocatalytic performances," *Langmuir*, vol. 26, no. 9, pp. 6618–6624, 2010.

[27] P. Wang, B. B. Huang, X. Y. Qin, X. Y. Zhang, Y. Dai, and M. H. Whangbo, "Ag/AgBr/$WO_3 \cdot H_2O$: visible-light photocatalyst for bacteria destruction," *Inorganic Chemistry*, vol. 48, pp. 10697–10702, 2009.

[28] P. Wang, B. B. Huang, X. Y. Qin, X. Y. Zhang, Y. Dai, and M. H. Whangbo, "Ag/AgBr/$WO_3 \cdot H_2O$: visible-light photocatalyst for bacteria destruction," *Inorganic Chemistry*, vol. 48, pp. 10697–10702, 2009.

[29] L. Zhang, K.-H. Wong, Z. Chen et al., "AgBr-Ag-Bi_2WO_6 nanojunction system: a novel and efficient photocatalyst with double visible-light active components," *Applied Catalysis A*, vol. 363, no. 1-2, pp. 221–229, 2009.

[30] L.-S. Zhang, K.-H. Wong, H.-Y. Yip et al., "Effective photocatalytic disinfection of E. coli K-12 using AgBr-Ag-Bi_2WO_6 nanojunction system irradiated by visible light: the role of diffusing hydroxyl radicals," *Environmental Science and Technology*, vol. 44, no. 4, pp. 1392–1398, 2010.

[31] M. Ge, N. Zhu, Y. Zhao, J. Li, and L. Liu, "Sunlight-assisted degradation of dye pollutants in Ag_3PO_4 suspension," *Industrial and Engineering Chemistry Research*, vol. 51, no. 14, pp. 5167–5173, 2012.

[32] J. J. Buckley, A. F. Lee, L. Olivi, and K. Wilson, "Hydroxyapatite supported antibacterial Ag_3PO_4 nanoparticles," *Journal of Materials Chemistry*, vol. 20, no. 37, pp. 8056–8063, 2010.

[33] G. F. Huang, Z. L. Ma, W. Q. Huang et al., "Ag_3PO_4 semiconductor photocatalyst: possibilities and challenges," *Journal of Nanomaterials*, Article ID 371356, pp. 1–8, 2013.

[34] R. H. Victora, "Calculated electronic structure of silver halide crystals," *Physical Review B*, vol. 56, no. 8, pp. 4417–4421, 1997.

[35] C. Shifu, Z. Wei, L. Wei, and Z. Sujuan, "Preparation, characterization and activity evaluation of p-n junction photocatalyst p-NiO/n-ZnO," *Journal of Sol-Gel Science and Technology*, vol. 50, no. 3, pp. 387–396, 2009.

[36] H. Zhang, G. Wang, D. Chen, X. Lv, and J. Li, "Tuning photoelectrochemical performances of Ag—TiO_2 nanocomposites via reduction/oxidation of Ag," *Chemistry of Materials*, vol. 20, no. 20, pp. 6543–6549, 2008.

[37] Y. Bi, S. Ouyang, J. Cao, and J. Ye, "Facile synthesis of rhombic dodecahedral AgX/Ag_3PO_4 (X = Cl, Br, I) heterocrystals with enhanced photocatalytic properties and stabilities," *Physical Chemistry Chemical Physics*, vol. 13, no. 21, pp. 10071–10075, 2011.

[38] W. Liu, M. Ji, and S. Chen, "Preparation, characterization and activity evaluation of $Ag_2Mo_4O_{13}$ photocatalyst," *Journal of Hazardous Materials*, vol. 186, no. 2-3, pp. 2001–2008, 2011.

[39] R. Jiang, H. Zhu, X. Li, and L. Xiao, "Visible light photocatalytic decolourization of C. I. Acid Red 66 by chitosan capped CdS composite nanoparticles," *Chemical Engineering Journal*, vol. 152, no. 2-3, pp. 537–542, 2009.

[40] J. Cao, B. Luo, H. Lin, and S. Chen, "Synthesis, characterization and photocatalytic activity of $AgBr/H_2WO_4$ composite photocatalyst," *Journal of Molecular Catalysis A*, vol. 344, no. 1-2, pp. 138–144, 2011.

[41] J. J. Liu, X. L. Fu, S. F. Chen, and Y. F. Zhu, "Electronic structure and optical properties of Ag_3PO_4 photocatalyst calculated by hybrid density functional method," *Applied Physics Letters*, vol. 99, no. 19, Article ID 191903, 2011.

[42] X. Zhang, L. Zhang, T. Xie, and D. Wang, "Low-temperature synthesis and high visible-light-induced photocatalytic activity of $BiOI/TiO_2$ heterostructures," *Journal of Physical Chemistry C*, vol. 113, no. 17, pp. 7371–7378, 2009.

[43] X. Huang, I. H. El-Sayed, W. Qian, and M. A. El-Sayed, "Cancer cell imaging and photothermal therapy in the near-infrared region by using gold nanorods," *Journal of the American Chemical Society*, vol. 128, no. 6, pp. 2115–2120, 2006.

[44] H. Liu, D. A. Genov, D. M. Wu et al., "Magnetic plasmon hybridization and optical activity at optical frequencies in metallic nanostructures," *Physical Review B*, vol. 76, no. 7, Article ID 073101, 2007.

[45] P. Wang, B. B. Huang, X. Y. Qin, X. Y. Zhang, Y. Dai, and M. Whangbo, "$Ag/AgBr/WO_3 \cdot H_2O$: visible-light photocatalyst for bacteria destruction," *Inorganic Chemistry*, vol. 48, pp. 10697–10702, 2009.

[46] C. Hu, Y. Lan, J. Qu, X. Hu, and A. Wang, "$Ag/AgBr/TiO_2$ visible light photocatalyst for destruction of azodyes and bacteria," *Journal of Physical Chemistry B*, vol. 110, no. 9, pp. 4066–4072, 2006.

[47] M. R. Elahifard, S. Rahimnejad, S. Haghighi, and M. R. Gholami, "Apatite-coated $Ag/AgBr/TiO_2$ visible-light photocatalyst for destruction of bacteria," *Journal of the American Chemical Society*, vol. 129, no. 31, pp. 9552–9553, 2007.

[48] K.-I. Ishibashi, A. Fujishima, T. Watanabe, and K. Hashimoto, "Detection of active oxidative species in TiO_2 photocatalysis using the fluorescence technique," *Electrochemistry Communications*, vol. 2, no. 3, pp. 207–210, 2000.

[49] Q. Xiao, Z. Si, J. Zhang, C. Xiao, and X. Tan, "Photoinduced hydroxyl radical and photocatalytic activity of samarium-doped TiO_2 nanocrystalline," *Journal of Hazardous Materials*, vol. 150, no. 1, pp. 62–67, 2008.

[50] X. F. Zhou, C. Hu, X. X. Hu, T. W. Peng, and J. H. Qu, "Plasmon-assisted degradation of toxic pollutants with $Ag–AgBr/Al_2O_3$ under visible-light irradiation," *The Journal of Physical Chemistry C*, vol. 114, pp. 2746–2750, 2010.